Nuclear Physics and Engineering (2018) 1(2):27–33

Nuclear Physics and Engineering

An International Peer-Reviewed Journal (http://npe.kntu.ac.ir)

Analysis of the fusion hindrance phenomenon for ^{58}Ni+^{54}Fe fusion reaction using cold nuclear matter properties

Reza Gharaei*

Department of Physics, Faculty of Science, Hakim Sabzevari University, P.O. Box 397, Sabzevar, Iran
*Corresponding author: r.gharaei@hsu.ac.ir

HIGHLIGHTS

- The saturation property of NM leads to appear a shallow pocket in the inner regions of the potential.
- Fusion hindrance phenomenon occurs at energies below $E_{c.m.} = 87.29$ MeV for ^{58}Ni+^{54}Fe colliding system.
- The incompressibility effects are responsible for describing the measured fusion cross sections of ^{58}Ni+^{54}Fe.
- Results show reasonable agreements with the experimental data of the $S(E)$ and $L(E)$ factors.

ABSTRACT

The role of saturation property of cold nuclear matter is examined in order to describe the steep falloff phenomenon of the measured fusion cross sections at energies far below the Coulomb barrier for ^{58}Ni+^{54}Fe colliding system. For this aim, the double-folding microscopic approach which is modified by modeling the repulsive core effects in the nucleon-nucleon interactions is used to calculate the nuclear interaction potential. Moreover, the theoretical values of the fusion cross section, S factor, and the logarithmic derivative are computed using the coupled-channel technique, including couplings to the low-lying 2^+ and 3^- states in target and projectile. The obtained results reveal that the corrective effects of cold nuclear matter can be responsible for the description of the fusion hindrance phenomenon in our chosen system.

KEYWORDS

Heavy-ion fusion reactions
Fusion hindrance
Phenomenon
Repulsive core effects
Double-folding model

1 Introduction

The study on the complete fusion channel of two interacting nuclei through both theoretical and experimental approaches has attracted considerable interest over the last decades. For example see Refs. (Jiang et al., 2002, 2004, 2006; Montagnoli et al., 2010a; Stefanini et al., 2010; Montagnoli et al., 2010b, 2012, 2013; Ghodsi and Gharaei, 2011, 2012a,b). In the experimental point of view, many efforts have been made to measure the fusion cross sections at various bombarding energies (Jiang et al., 2002, 2004, 2006; Montagnoli et al., 2010b; Stefanini et al., 2010; Montagnoli et al., 2012; Stefanini et al., 2015, 2013; Jiang et al., 2005). The recent progresses in the experimental techniques have enabled us to extend these measurements to the energies well below the fusion barrier (sub-μb levels).

The experimental findings for several medium-heavy mass systems at low energies reveal that the measured fusion cross sections falloff steeply with respect to the standard "coupled-channel (CC)" calculations (Hagino et al., 1999). This unexpected behavior, which was observed for the first time in the fusion of ^{60}Ni with ^{89}Y (Jiang et al., 2002), is known as fusion hindrance phenomenon. According to the literature, two theoretical approaches can be used to explain this phenomenon; One is the adiabatic approach introduced in Refs. (Ichikawa et al., 2007; Ichikawa, 2009, 2015), at which the characteristics of fusion process are modeled when touching and overlapping of the reacting partner, and the other is the proposed approach in Refs. (Mişicu and Esbensen, 2006, 2007; Esbensen and Mişicu, 2007) which is based on the sudden approximation of the density distributions and also the saturation properties of nuclear matter (NM).

Fusion of ^{58}Ni projectile with ^{54}Fe target is a new fusion system with negative Q-value ($Q = -56.45$ MeV). Measurements of the excitation functions for this fusion system have been reported by Stefanini *et al.* (Stefanini

Article history: Received 30 Sept 2017/ Revised manuscript received 14 April 2018/ Accepted 4 May 2018/ Available online 1 July 2018

et al., 2010). In that study, the reported fusion cross sections are measured down to 1 μb. It should be noted that the ^{58}Ni projectile and the ^{54}Fe target have closed proton and neutron shells, respectively. In other words, they are stiff nuclei. Stefanini *et al.* (Stefanini et al., 2010) observed a clear maximum in the energy-dependent trend of the experimental data of the astrophysical S-factor. One can therefore confirm the appearance of fusion hindrance phenomenon in the colliding system ^{58}Ni+^{54}Fe (Stefanini et al., 2010, 2015). From the theoretical point of view, several efforts have been made to reproduce the experimental fusion cross sections especially at low incident energies of ^{58}Ni projectile. It is shown that the CC calculations even with a phenomenological diffuse ($a = 0.90$ fm) (Stefanini et al., 2010) or deep ($V_0 = 101.16$ MeV) (Stefanini et al., 2015) nuclear potential are fail to reproduce the steep fall-off of the measured fusion cross sections of ^{58}Ni+^{54}Fe. Under these conditions, the presentation of a suitable theoretical framework can be quite useful for analyzing the energy-dependent behavior of the fusion data in the considered reaction.

In the present work, for the first time an effort is made to address the influence of the cold NM properties on the ^{58}Ni+^{54}Fe fusion system using the proposed procedure of Refs. (Mişicu and Esbensen, 2006, 2007). According to these studies, one needs to simulate the repulsive core effects in the nucleon-nucleon (NN) interactions and then calculate the strength of the nuclear interactions during the fusion process within the framework of double-folding (DF) model. We carry out the calculations of the theoretical values of the fusion cross sections based on the CC approach (Hagino et al., 1999). In these calculations, the couplings to the low-lying 2^+ and 3^- states are considered for both target and projectile nuclei. We also explore the energy-dependent trend of the astrophysical $S(E)$ factor and the exponential slope of the excitation function $L(E)$ as two widely used quantities in the context of fusion hindrance studies. It is remarkable that in the S-factor representation, a maximum in experimental values of this factor appears for all systems with negative fusion Q-values, whereas the experimental values of $L(E)$ increase by decreasing the bombarding energy.

This paper is organized as follows: The potential models for calculating the strength of nuclear interactions during the fusion process are described in Sec. 2. Section 3 is devoted to the analysis of the obtained results for the interaction potentials and fusion cross sections as well. In this section, we also present the results of the $S(E)$ factor and logarithmic derivative $L(E)$ for fusion of ^{58}Ni+^{54}Fe. The main results obtained are remarked in Sec. 4.

2 Details of calculations

As stated earlier, the main purpose of the present study is to explain the steep falloff phenomenon of the sub-barrier fusion cross sections for ^{58}Ni+^{54}Fe $\rightarrow^{112}$Xe* colliding system with $Q = -56.45$ MeV. Aage-Winther (AW) potential (Winther, 1995) is a standard form of the ion-ion potential which is commonly used for evolution of the mentioned phenomenon in heavy-ion fusion reactions with negative $Q-$values; for example see Ref. (Ramezani and Ghodsi, 2014). This semi-empirical potential model can be defined in the form of a Woods-Saxon parameterization as (Winther, 1995):

$$V_N^{\rm AW}(r) = -\frac{V_0}{1+\exp(\frac{\rm r-R_0}{a})} \quad \text{MeV}, \tag{1}$$

where the parameters of the depth V_0, radius R_0 and diffuseness a are given by

$$V_0 = 16\pi\frac{R_1R_2}{R_1+R_2}\gamma a \quad \text{MeV}, \tag{2}$$

$$R_0 = R_1 + R_2, \tag{3}$$

$$a = \left[\frac{1}{1.17(1+0.53(A_1^{-1/3}+A_2^{-1/3}))}\right] \quad \text{fm}. \tag{4}$$

In this model, the radius parameter R_i can be defined as

$$R_i = 1.20A_i^{1/3} - 0.09 \quad \text{fm} \qquad (i = 1, 2). \tag{5}$$

In addition, γ is the surface energy coefficient and is given by

$$\gamma = \gamma_0\left[1 - k_s\left(\frac{N_P - Z_P}{A_P}\right)\left(\frac{N_T - Z_T}{A_T}\right)\right], \tag{6}$$

where $\gamma_0 = 0.95$ MeV/fm^2 and $k_s = 1.8$. Moreover, $N_{P(T)}$, $Z_{P(T)}$ and $A_{P(T)}$ are the number of neutrons, the number of protons and the number of nucleons of the projectile and target, respectively. Considering the literature, while AW potential provides reliable Coulomb barrier, it cannot reproduce the fusion data at energies far below the barrier. In other words, this form of ion-ion potential produces pockets that are too deep in the part of the barrier.

In the second step, we use the DF technique to calculate the nuclear potential between two reacting nuclei. According to Refs. (Satchler and Love, 1979; Khoa and Satchler, 2000), this microscopic potential can be defined as

$$V_{DF}(\mathbf{R}) = \int d\mathbf{r}_1 \int d\mathbf{r}_2 \rho_1(\mathbf{r}_1)\rho_2(\mathbf{r}_2)\upsilon_{NN} \qquad (\mathbf{r}_{12} = \mathbf{R} + \mathbf{r}_2 - \mathbf{r}_1). \tag{7}$$

Equation (7) consists of two main inputs:

i. The density distribution, $\rho_i(\mathbf{r}_i)$, of the target and projectile nuclei. Here, we have used two-parameter Fermi-Dirac (2PF) distribution function:

$$\rho_{\rm 2PF}(r) = \frac{\rho_0}{1+\exp\left[(r-R_0)/a_0\right]}, \tag{8}$$

and three-parameter Fermi-Dirac (3PF) distribution function:

$$\rho_{\rm 3PF}(r) = \frac{\rho_0(1+\omega r^2/R_0^2)}{1+\exp\left[(r-R_0)/a_0\right]}, \tag{9}$$

for parameterization of the density in the ^{54}Fe target and the ^{58}Ni projectile, respectively. The parameters correspond to these profiles are extracted from the electron scattering experiments (De Vries et al., 1987) (See Table 1).

ii. The effective NN interactions υ_{NN}. In the present study, this part is parameterized by the M3Y-Paris effective interaction (Bertsch et al., 1977).

Due to the fact that the M3Y-DF potential is much deeper than the ground state energy of the compound nucleus formed during the fusion process, one can find out this form of the nuclear potential is unrealistic at short distances between two reacting nuclei. To cure this deficiency, the M3Y interaction has been corrected by supplementing it with a repulsion term as $\upsilon_{\rm rep}(\mathbf{r}_{12}) = V_{\rm rep}\delta(\mathbf{r}_{12})$ (Mişicu and Esbensen, 2006, 2007). The existence of this short-ranged potential can be attributed to the presence of the Pauli exclusion principle in the NN interactions. The strength of the repulsive core potential can be estimated by substituting the suggested form $\upsilon_{\rm rep}(\mathbf{r}_{12})$ for the central part of the DF integral, Eq. (7), as follows:

$$V_{\rm rep}(\mathbf{R}=\mathbf{0}) = \int {\rm d}\mathbf{r}_1 \int {\rm d}\mathbf{r}_2 \rho_1(\mathbf{r}_1) V_{\rm rep}\delta(\mathbf{r}_{12})\rho_2(\mathbf{r}_2). \quad (10)$$

It is worthy to mention that the calculations of the repulsive core potential are performed within the complete overlapping region of density distribution, namely at internuclear distance $R = 0$. Moreover, for taking into account the surface diffuseness effects of these reacting nuclei during overlapping process, it is assumed that the diffuseness parameter in the density distributions of target and projectile equal $a_{\rm rep}$ (Mişicu and Esbensen, 2006, 2007). Under these conditions, we will deal with two adjustable parameters $V_{\rm rep}$ and $a_{\rm rep}$ for simulating the repulsive core effects. The proposed procedure of Mişicu and Esbensen (Mişicu and Esbensen, 2007) is employed for calculating and choosing these parameters. In the present study, the theoretical results of the modified form of the M3Y-DF model using the repulsive core effects are marked as "M3Y+Repulsion" model.

3 Results and discussion

In the first step, we intend to analyze the radial behavior of the total interaction potential for ^{58}Ni+^{54}Fe colliding system based on the AW and M3Y-DF models. The calculated potentials are shown in Fig. 1. The AW potential parameters used are $V_0 = 71.73$ MeV, $R_0 = 1.17$ fm and $a = 0.67$ fm. The height of the Coulomb barrier generated by this potential model is $V_B = 92.96$ MeV, whereas the barrier height obtained from the M3Y-DF model is lower ($V_B = 91.32$ MeV). This difference is quite evident from Fig. 1. Moreover, it is shown that the interaction potential based on the pure M3Y-DF model obeys an unphysical behavior at shorter distances between ^{58}Ni and ^{54}Fe nuclei. In fact, this model predicts that the potential is much deeper than the ground-state energy of the compound nucleus ^{112}Xe* in the inner region of the barrier.

Table 1: The parameters used for the density distributions of the ^{58}Ni projectile and ^{54}Fe target nuclei. The values are taken from Ref. (De Vries et al., 1987).

Nucleus	Profile	R_0 (fm)	a_0 (fm)	ω
^{58}Ni	3PF	4.309(2)	0.516(9)	-0.1308
^{54}Fe	2PF	4.074(14)	0.536(6)	–

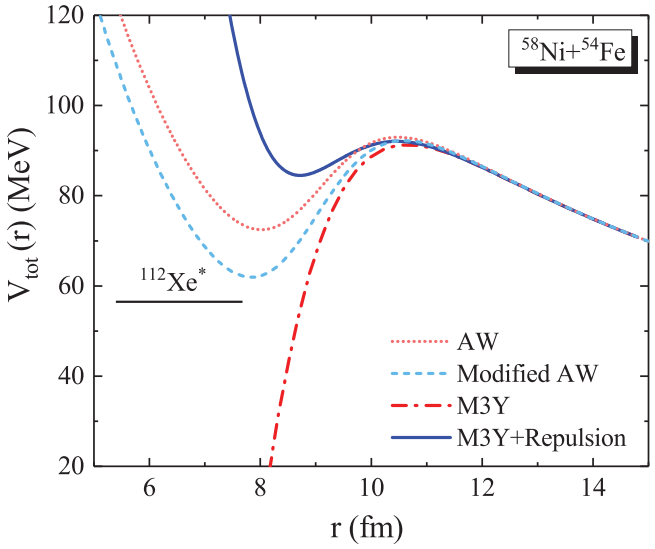

Figure 1: Comparison of the M3Y-DF potentials (with and without repulsion effects) with the original and modified forms of the AW potential for the ^{58}Ni+^{54}Fe colliding system. The energy of the ground state of the compound nucleus ^{112}Xe* (lower horizontal line) is also indicated.

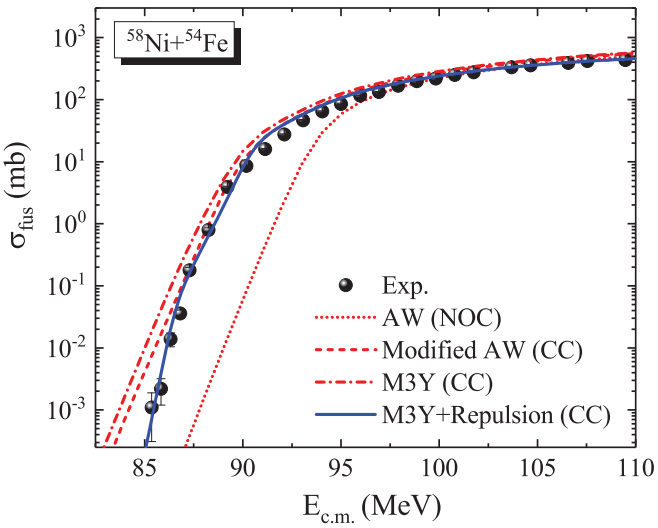

Figure 2: Fusion cross sections for ^{58}Ni+^{54}Fe system as a function of center-of-mass energy $E_{\rm c.m.}$ (in MeV). The dotted line denotes the result of single-channel calculations (no-couplings) with the original form of the AW potential. The dashed and dash-dotted curves represent the results of CC calculations based on the modified form of AW and pure M3Y-Df model, respectively. The solid line denotes the result of the CC calculations with M3Y+Repulsion potential.

Figure 2 shows the energy-dependent behavior of the calculated and measured values of the fusion cross section for fusion system ^{58}Ni+^{54}Fe. It should be noted that the analytical calculations of this quantity are initially based on the one-dimensional barrier penetration model (1-DBPM) (Balantekin and Takigawa, 1998). In this model, the separation distance between target and projectile is considered as the only degree of freedom of fusion system. It is well known that this theoretical model enables us to provide acceptable description for the heavy-ion fusion cross sections measured at near and above barrier energies; For example see Refs. (Hagino and Takigawa, 2012; Gharaei, 2017). This subject is quite evident from the results of the 1-DBPM based on the original version of the AW potential (dotted lines) for ^{58}Ni+^{54}Fe colliding system shown in Fig. 2. However, this figure shows that the used approach cannot reproduce the experimental fusion cross sections at sub-barrier energies. In order to achieve more accurate results in these energy regions we here employ two following solutions:

i. It is well known that the reduction of the Coulomb barrier height plays a significant role in increasing the fusion probability and resulting the fusion cross section. We therefore increase the strength of the nuclear potential based on the AW model by changing the value of depth parameter from $V_0 = 71.73$ MeV to $V_0 = 85.50$ MeV, where the radius R_0 and diffuseness parameter a are the same as in the original version of this potential. Such a change leads to decrease the Coulomb barrier height as much as 0.77 MeV.

ii. It is now realized that the CC approach leads to an enhancement of the sub-barrier fusion cross sections (Balantekin and Takigawa, 1998; Dasgupta et al., 1998; Beckerman, 1988; Steadman and Rhoades-Brown, 1986; Reisdorf, 1994; Stokstad et al., 1980; Leigh et al., 1995). In this approach, the coupling effects of the relative motion of the colliding nuclei to nuclear intrinsic motions (such as the rotational and vibrational modes) are taken into account. In the present study, we include the coupling to the low-lying 2^+ and 3^- states in target and projectile. Moreover, the exact CC calculations have been performed using the computer code CCFULL (Hagino et al., 1999). The nuclear structure inputs of quadrupole and octupole states for our selected reacting nuclei are given in Table 2.

Table 2: Structure inputs of low-lying excited states in ^{58}Ni projectile and ^{54}Fe target, including the excitation energies E^*, reduced transition probabilities $B(E\lambda)$ and deformation parameters β_λ, which are extracted from the literature (Raman et al., 1989; Kibedi and Spear, 2002).

Nucleus	λ^π	E^* (MeV)	$B(E\lambda)$(e^{2}b$^\lambda$)	β_λ
^{58}Ni	2^+	1.454	0.0698	0.1828
	3^-	4.475	0.0176	0.198
^{54}Fe	2^+	1.408	0.062	0.195
	3^-	4.782	0.0044	0.115

Table 3: The parameters $a_{\rm rep}$ and $V_{\rm rep}$ used in modeling the repulsive core effects for fusion of ^{58}Ni+^{54}Fe. The obtained values for the nuclear matter incompressibility constant K and the pocket energy $V_{\rm pocket}$ are also presented.

Reaction	$a_{\rm rep}$ (fm)	$V_{\rm rep}$ (MeV fm^3)	K (MeV)	$V_{\rm pocket}$ (MeV)
^{58}Ni+^{54}Fe	0.375	527.1	233.94	84.33

By computing the theoretical values of the fusion cross sections using the CC calculations based on the modified form of the AW potential (dashed line in Fig. 2), we would obtain more accurate results for ^{58}Ni+^{54}Fe reaction, especially at low incident energies. In other words, there is reasonable agreement with the experimental data at energies above the $E_{\rm c.m.} = 87.29$ MeV. This energy refers to the onset of the fusion hindrance phenomenon in the case of ^{58}Ni+^{54}Fe colliding system (Stefanini et al., 2010). For lower bombarding energies, a steep increase at the measured cross sections takes place. Figure 2 also compares the experimental fusion cross sections for ^{58}Ni+^{54}Fe with those calculated using CC approach based on the M3Y-DF model. The obtained results reveal that this model overestimates the fusion data at the whole range of energy. To improve the curve fitted to the data, we impose the corrective effects of the cold NM incompressibility on the standard M3Y heavy-ion potential. The obtained values of the parameters used in modeling the repulsive core effects ($a_{\rm rep}$ and $V_{\rm rep}$) along with the associated incompressibility constant K and pocket energy $V_{\rm Pocket}$ are listed in Table 3 for fusion of ^{58}Ni with ^{54}Fe.

For our arbitrary chosen fusion reaction, the interaction potential calculated by the M3Y+Repulsion model is shown in Fig. 1. It can be seen that the imposing of these corrective effects leads to appearing a shallow pocket in the inner regions of the barrier. In this figure, we have also compared the radial behavior of the interaction potential obtained by using the M3Y+Repulsion model with that of the modified form of the AW model. It can be find out that the pocket predicted by the M3Y+repulsion potentials is much shallower than predicted by the AW potential. The solid line in Fig. 2 shows the fusion cross sections obtained by the CC calculations based on the modified form of the M3Y-DF potential. It is shown that a repulsive potential which takes into account the incompressibility of the nuclear matter can reproduce the measured fusion cross sections of ^{58}Ni+^{54}Fe in the sub-μb range with an acceptable accuracy.

The astrophysical $S(E)$ factor is one of the favorable quantities which can be helpful for analyzing the fusion hindrance phenomenon. One can define this factor in terms of the fusion cross section as (Jiang et al., 2014):

$$S(E) = E\sigma_{\rm fus}\exp[2\pi(\eta - \eta_0)], \qquad (11)$$

where $\eta = e^2 Z_p Z_t/\hbar v_{\rm rel}$ is the Sommerfeld parameter and $v_{\rm rel}$ is the relative velocity between the target and projectile in the center-off-mass frame. Moreover, η_0 is an adjustable parameter. As mentioned earlier, for medium-heavy systems with negative Q-values, the experimental

data of the $S(E)$ factor develop a maximum value at deep sub-barrier energies. It is claimed that the onset of fusion hindrance corresponds to bombarding energy at which the S-factor reaches its maximum value. This energy is marked as $E_s^{\text{exp.}}$.

The $S(E)$ factor representation for the ^{58}Ni+^{54}Fe fusion system is presented in Fig. 3. In this figure, the theoretical values calculated by various potential models are compared with the corresponding experimental data of $S(E)$. Here, we take $\eta_0 = 60.00$. A clear maximum appears in the experimental trend of this factor at energy $E_s^{\text{exp.}} = 87.29$ MeV. From the theoretical point of view, the results obtained from Fig. 3 reveal that the original and modified forms of the AW potential, and the pure M3Y-DF model as well, can not reproduce the energy-dependent behavior of $S(E)$ factor at sub-barrier energies. However, the corrective effects imposed on the AW potential play an important role in increasing the accuracy of the associated calculations of this factor at low energies. The solid curve in Fig. 3 is based on the CC calculations with M3Y+Repulsion potential. It is shown that these calculations provide an excellent description of the data.

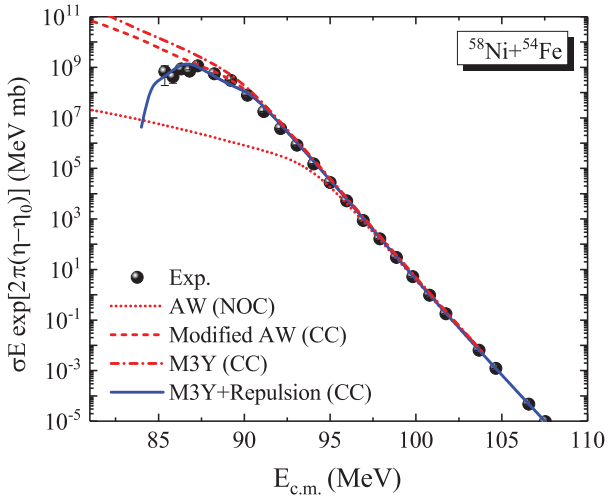

Figure 3: Same as Fig. 2 but for the energy-dependent behavior of the astrophysical $S(E)$ factor.

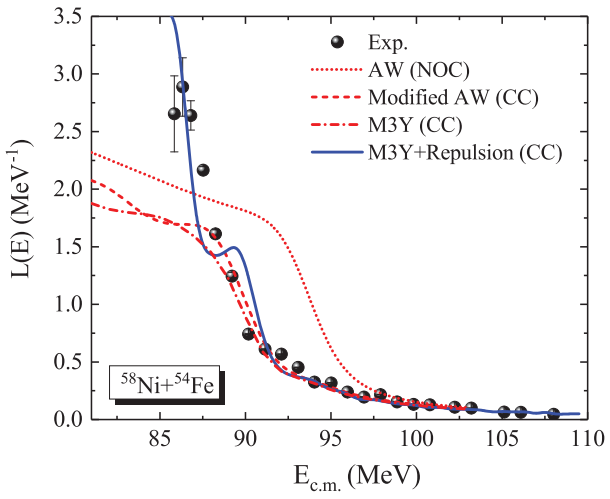

Figure 4: Same as Fig. 2 but for the energy-dependent behavior of the logarithmic derivative $L(E)$ factor.

To achieve further understanding from the behavior of sub-barrier fusion cross sections, one can use the logarithmic derivative $L(E)$. This quantity can be defined as

$$L(E) = \frac{\mathrm{d}[\ln(E\sigma_{\text{fus}})]}{\mathrm{d}E} = \frac{1}{E\sigma_{\text{fus}}}\frac{\mathrm{d}(E\sigma_{\text{fus}})}{\mathrm{d}E}. \qquad (12)$$

Here, we have calculated the theoretical values of $L(E)$ factor using various potential models considered for ^{58}Ni+^{54}Fe fusion reaction. A comparison with the corresponding experimental data is given in Fig. 4. Obviously, the experimental values of the exponential slope $L(E)$ keep their increasing trend by decreasing energy down to the lowest incident energy. However, the original and modified forms of the AW potential, and the pure M3Y-DF model as well, predict that the theoretical values of $L(E)$ are saturated at energies under the Coulomb barrier. Another point to note in this figure is that a reasonable agreement with the available experimental data is obtained for the M3Y-DF model accompanied by the "CC calculations + cold NM incompressibility effects".

4 Concluding remarks

In summary, we have tried to analyze the importance of the cold NM incompressibility effects on the reproduction of the measured fusion cross sections of the ^{58}Ni+^{54}Fe reaction (with $Q < 0$), especially at extreme sub-barrier energies. To achieve this aim, we have modeled the repulsive core effects in the NN interactions using the DF microscopic potential model. We have also calculated the total interaction potential based on the modified form of the standard AW potential model. The calculations of the fusion cross sections, the S factor and the logarithmic derivative $L(E)$ are based on the CC approach which includes the coupling to the lowest 2^+ and 3^- states in target and projectile.

The main results obtained in the present study can be summarized as follow:

- Comparison of the M3Y-DF potentials with and without the repulsive core effects reveal that the imposing of the saturation property of cold NM on the calculations of the interaction potential of ^{58}Ni+^{54}Fe reaction leads to appearing a shallow pocket in the inner region of the fusion barrier. In addition, our calculations show that the pocket produced by M3Y+Repulsion potential is much shallower than that of the AW potential.

- We found out that the modified form of the AW model enables us to reproduce the experimental data of the fusion cross section only for energies above $E_{\text{c.m.}} = 87.29$ MeV. This result is also valid for the energy-dependent behaviors of the $S(E)$ and $L(E)$ factors in the ^{58}Ni+^{54}Fe colliding system.

- It has been shown that the saturation effects of cold NM can be responsible for the description of fusion hindrance phenomenon in our selected reaction. In other words, an acceptable agreement is obtainable between the theoretical and experimental values of

$\sigma(E)$, $S(E)$ and $L(E)$ quantities, especially at sub-barrier energies using the CC calculations which are based on the M3Y+Repulsion potential.

References

Balantekin, A. B. and Takigawa, N. (1998). Quantum tunneling in nuclear fusion. *Reviews of Modern Physics*, 70(1):77.

Beckerman, M. (1988). Sub-barrier fusion of two nuclei. *Reports on Progress in Physics*, 51(8):1047.

Bertsch, G., Borysowicz, J., McManus, H., et al. (1977). Interactions for inelastic scattering derived from realistic potentials. *Nuclear Physics A*, 284(3):399–419.

Dasgupta, M., Hinde, D. J., Rowley, N., et al. (1998). Measuring barriers to fusion. *Annual Review of Nuclear and Particle Science*, 48(1):401–461.

De Vries, H., De Jager, C., and De Vries, C. (1987). Nuclear charge-density-distribution parameters from elastic electron scattering. *Atomic Data And Nuclear Data Tables*, 36(3):495–536.

Esbensen, H. and Mişicu, Ş. (2007). Hindrance of ^{16}O+^{208}Pb fusion at extreme sub-barrier energies. *Physical Review C*, 76(5):054609.

Gharaei, R. (2017). Analysis of the low-and high-energy fusion cross sections: the case of ^{58}Ni+^{54}Fe. *Journal of Physics G: Nuclear and Particle Physics*, 44(4):045108.

Ghodsi, O. N. and Gharaei, R. (2011). Equation of state of hot polarized nuclear matter and heavy-ion fusion reactions. *Physical Review C*, 84(2):024612.

Ghodsi, O. N. and Gharaei, R. (2012a). Temperature dependence of the repulsive core potential in heavy-ion fusion reactions. *Physical Review C*, 85(6):064620.

Ghodsi, O. N. and Gharaei, R. (2012b). The study of the nucleus–nucleus interaction potential for ^{16}O+^{27}Al and ^{16}O+^{28}Si fusion reactions. *Modern Physics Letters A*, 27(06):1250037.

Hagino, K., Rowley, N., and Kruppa, A. T. (1999). A program for coupled-channel calculations with all order couplings for heavy-ion fusion reactions. *Computer Physics Communications*, 123(1-3):143–152.

Hagino, K. and Takigawa, N. (2012). Subbarrier fusion reactions and many-particle quantum tunneling. *Progress of Theoretical Physics*, 128(6):1061–1106.

Ichikawa, T. (2009). T. Ichikawa, K. Hagino, and A. Iwamoto, Phys. Rev. Lett. 103, 202701 (2009). *Physical Review Letters*, 103:202701.

Ichikawa, T. (2015). Systematic investigations of deep subbarrier fusion reactions using an adiabatic approach. *Physical Review C*, 92(6):064604.

Ichikawa, T., Hagino, K., and Iwamoto, A. (2007). Existence of a one-body barrier revealed in deep subbarrier fusion. *Physical Review C*, 75(5):057603.

Jiang, C. L., Back, B. B., Esbensen, H., et al. (2006). First evidence of fusion hindrance for a small Q-value system. *Physics Letters B*, 640(1-2):18–22.

Jiang, C. L., Esbensen, H., Rehm, et al. (2002). Unexpected behavior of heavy-ion fusion cross sections at extreme sub-barrier energies. *Physical Review Letters*, 89(5):052701.

Jiang, C. L., Rehm, K. E., Esbensen, H., et al. (2005). Hindrance of heavy-ion fusion at extreme sub-barrier energies in open-shell colliding systems. *Physical Review C*, 71(4):044613.

Jiang, C. L., Rehm, K. E., Janssens, R., et al. (2004). Influence of nuclear structure on sub-barrier hindrance in Ni+Ni fusion. *Physical Review Letters*, 93(1):012701.

Jiang, C. L., Stefanini, A. M., Esbensen, H., et al. (2014). Fusion hindrance for a positive-Q-value system ^{24}Mg+^{30}Si. *Physical Review Letters*, 113(2):022701.

Khoa, D. T. and Satchler, G. R. (2000). Generalized folding model for elastic and inelastic nucleus–nucleus scattering using realistic density dependent nucleon–nucleon interaction. *Nuclear Physics A*, 668(1-4):3–41.

Kibedi, T. and Spear, R. H. (2002). Reduced electric-octupole transition probabilities, B(E3;01+→31-) -An update. *Atomic Data and Nuclear Data Tables*, 80(1):35–82.

Leigh, J., Dasgupta, M., Hinde, D., et al. (1995). Barrier distributions from the fusion of oxygen ions with ^{144,148,154}Sm and ^{186}W. *Physical Review C*, 52(6):3151.

Mişicu, Ş. and Esbensen, H. (2006). Hindrance of heavy-ion fusion due to nuclear incompressibility. *Physical Review Letters*, 96(11):112701.

Mişicu, Ş. and Esbensen, H. (2007). Signature of shallow potentials in deep sub-barrier fusion reactions. *Physical Review C*, 75(3):034606.

Montagnoli, G., Scarlassara, F., Mason, P., et al. (2010a). Sub-barrier fusion hindrance in medium-light systems. *Nuclear Physics A*, 834(1-4):159c–162c.

Montagnoli, G., Stefanini, A. M., Corradi, L., et al. (2010b). Sub-barrier fusion of ^{36}S+^{64}Ni and other medium-light systems. *Physical Review C*, 82(6):064609.

Montagnoli, G., Stefanini, A. M., Esbensen, H., et al. (2013). Effects of transfer channels on near-and sub-barrier fusion of ^{32}S+^{48}Ca. *Physical Review C*, 87(1):014611.

Montagnoli, G., Stefanini, A. M., Jiang, C. L., et al. (2012). Fusion of ^{40}Ca+^{40}Ca and other Ca+Ca systems near and below the barrier. *Physical Review C*, 85(2):024607.

Raman, S., Nestor J r, C. W., Kahane, S., et al. (1989). Predictions of B(E2;01+→21+) values for even-even nuclei. *Atomic Data and Nuclear Data Tables*, 42(1):1–54.

Ramezani, M. and Ghodsi, O. N. (2014). Analysis of the fusion excitation functions for the ^{28}Si+^{94}Mo, 100 systems. *Physical Review C*, 89(3):034006.

Reisdorf, W. (1994). Heavy-ion reactions close to the Coulomb barrier. *Journal of Physics G: Nuclear and Particle Physics*, 20(9):1297.

Satchler, G. R. and Love, W. G. (1979). Folding model potentials from realistic interactions for heavy-ion scattering. *Physics Reports*, 55(3):183–254.

Steadman, S. G. and Rhoades-Brown, M. J. (1986). Subbarrier fusion reactions. *Annual Review of Nuclear and Particle Science*, 36(1):649–681.

Stefanini, A. M., Montagnoli, G., Corradi, L., et al. (2010). Fusion hindrance for ^{58}Ni+^{54}Fe. *Physical Review C*, 82(1):014614.

Stefanini, A. M., Montagnoli, G., Corradi, L., et al. (2015). Fusion of ^{48}Ti+^{58}Fe and ^{58}Ni+^{54}Fe below the Coulomb barrier. *Physical Review C*, 92(6):064607.

Stefanini, A. M., Montagnoli, G., Scarlassara, F., et al. (2013). Fusion of ^{60}Ni+^{100}Mo near and below the Coulomb barrier. *The European Physical Journal A*, 49(5):63.

Stokstad, R., Eisen, Y., Kaplanis, S., Pelte, D., Smilansky, U., and Tserruya, I. (1980). Fusion of ^{16}O + ^{148,150,152,154}Sm at sub-barrier energies. *Physical Review C*, 21(6):2427.

Winther, A. (1995). Dissipation, polarization and fluctuation in grazing heavy-ion collisions and the boundary to the chaotic regime. *Nuclear Physics A*, 594(2):203–245.